Surface Plasmon Microscopy Using an Energy-Filtered Low Energy Electron Microscope

Y. Fujikawa and T. Sakurai
Institute for Materials Research, Tohoku University, Sendai 980-8577, Japan

R. M. Tromp
IBM Research Division, T.J. Watson Research Center, 1101 Kitchawan Road, P.O. Box 218, Yorktown Heights, New York 10598, USA

(Received 19 September 2007; revised manuscript received 12 February 2008; published 25 March 2008)

We present low energy electron microscope (LEEM) spectromicroscopy studies of surface plasmons, localized on micro- and nanoscale epitaxial Ag islands. Excellent agreement is found in a direct comparison of wave vector dependent plasmon intensity with theory, demonstrating that high quality quantitative data can be obtained with a large improvement in both spatial and temporal resolution over traditional electron scattering experiments. The plasmon signal from Ag islands is successfully imaged with a spatial resolution of less than 35 nm. LEEM based plasmon spectromicroscopy promises to be a powerful tool for furthering our understanding of nanoplasmonics.

DOI: 10.1103/PhysRevLett.100.126803 PACS numbers: 73.20.Mf, 68.37.Nq, 73.22.Lp

Optical manifestations of surface plasmons (SP), such as Mie resonance [1] and surface enhanced Raman scattering [2], have long been studied intensively because their characteristic wavelength and the strength of the resonance can be controlled by the geometry of the metallic system mediating the plasmon. Important applications such as subwavelength optics [3], optoelectronics [4], single-molecule detection [5], and selective tumor therapy [6], have seen much recent process with advances in nanoscale structure control and analysis. Further developments in this field demand more detailed and quantitative investigations on the correlation between local structure and plasmonic property of the metallic system.

Real space observation of SP resonance effects has been achieved using optical scanning probe techniques [3,7] and photon detection in scanning tunneling microscopy [8]. Time resolved imaging of SP dynamics has been realized with two-photon photoemission in conjunction with photoemission electron microscopy (PEEM) [9]. These techniques give direct information on the optical SP resonances, but contain less information on the SP itself because optical probes excite the surface plasmon polariton rather than SP itself.

Electron energy loss spectroscopy (EELS), with response functions of $\mathrm{Im}(-1/\varepsilon)$ for bulk loss and $\mathrm{Im}\{-1/(1+\varepsilon)\}$ for surface loss (ε: dielectric function) gives direct information on bulk and surface plasmons, resulting in loss peaks at $\mathrm{Re}\varepsilon = 0$ and -1, respectively, corresponding to the excitation conditions for these plasmons. EELS combined with transmission electron microscopy (TEM) has been used for nanoscale imaging of the local plasmon distribution in metallic precipitates [10]. The field expansion of free-electron SP for a system comprising a flat surface and a sphere, as well as SP coupling between two spheres has been measured with $\sim$10 nm spatial resolution [11]. Although TEM has good sensitivity for both bulk and surface modes, the bulk part tends to be dominant with the electron energy (>100 keV) typically used in TEMs. Furthermore, the dielectric functions of metals such as Ag and Au, generally used for plasmonics due to superior response to visible light, are strongly modified by d-band excitations, resulting in the bulk and surface plasmon energies being very similar in the case of Ag [12]. In order to investigate such SPs with high spatial and spectroscopic resolution, energy-filtered microscopes working at much lower energy (<100 eV), i.e., low energy electron microscopes (LEEM), [13] are desirable to enhance the surface scattering.

In this Letter, we report energy-filtered imaging, as well as area-selected spectroscopy of SPs using the IBM LEEM-II low energy electron microscope [14] equipped with an in-line energy filter [15]. The SP energy vs momentum (E-Q) dispersion was obtained with $\sim$0.3 eV resolution from a 6 μm diameter area on a Ag(111) island grown on Si(111). The Q dependence of the peak intensity is in excellent agreement with classical scattering theory, demonstrating that high quality quantitative data can be obtained even from small samples. Energy-filtered real space SP loss images of a mixed Ag(111)-Ag(100) island on Si(111) show that the loss intensity is almost proportional to the electron reflectivity, as expected from electron scattering theory. Plasmon loss images of Ag nanostructures on Si(001) show that clusters of $\sim$40 nm diameter and $\sim$7 nm thickness are readily resolved in the image.

All experiments were carried out in the IBM LEEM-II system [14] with a base pressure of 1×10^{-10} Torr. Energy filter slits with widths of 1.5, 10, and 20 μm are installed in the diffraction plane between the transfer lens and the prism array beam deflector. Because of the chromatic dispersion of the prism array (9 μm/eV for 10 keV electrons), the electrons are dispersed linearly in energy in the conjugate diffraction plane behind the prism array (see the inset in Fig. 1), forming a direct image of the E-Q distribution, as described in detail elsewhere [15].

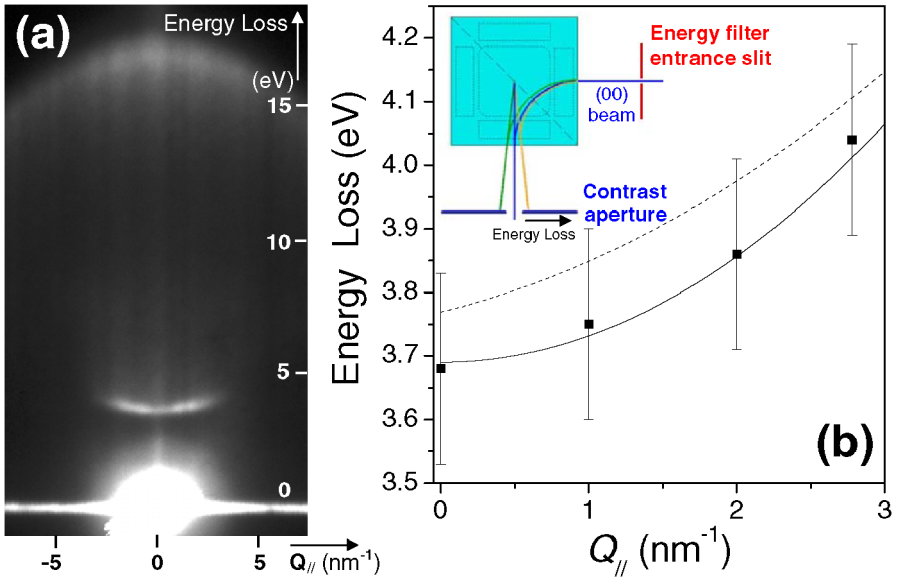

FIG. 1 (color online). (a) A typical electron energy loss spectrum obtained from a Ag(111) island with $E_I = 19$ eV. The slit is parallel to the $\bar{\Gamma} - \bar{\mathrm{M}}$ direction. Elastically scattered electrons form a bright band at $E_{\mathrm{loss}} = 0$, with the specular beam at $Q_{\parallel} = 0$. A SP loss feature is seen at 3.7–4.0 eV with noticable dispersion. (b) E-$Q_{\parallel}$ dispersion of the SP loss peak in Fig. 1(a). The energy width of the primary peak is indicated by error bars. Solid and broken lines represent fits for bulk [17] and thin film [20] Ag. The thin film dispersion (for a 13 ML thick film) is blue shifted due to thin film confinement effects. For the 50 nm thick film studied here, the dispersion is close to the bulk value. The inset to (b) shows how different energy electrons are dispersed in the exit plane of the prism array. Electrons with momentum normal to the figure plane are passed by the slit, to form an E-$Q_{\parallel}$ image in the exit plane. The contrast aperture is inserted for energy-filtered imaging only.

Flat Ag islands were grown on Si(111) substrate after converting the Si(111) clean surface to the $(\sqrt{3} \times \sqrt{3})$-Ag structure at 800 K, keeping the Ag flux at ~0.3 ML/min for 10 min. without substrate heating. This results in low density ($<10^{-4}/\mu\mathrm{m}^2$), large islands of ~20 μm diameter and ~50 nm thickness. Most islands exhibit the Ag(111) face, while some also contain rotated Ag(100) domains. Ag was also deposited with a flux of ~1 ML/min on Si(001) at 750 K for 12 min to form nanoclusters, after which the temperature was raised to 850 K for 23 min to obtain larger nanowires, coexisting with smaller nanoclusters. Island sizes are verified by conventional atomic force microscopy.

Energy-filtered experiments were performed by allowing both the incoming 10 keV electron beam and the reflected (00) LEED beam to pass through the energy filter slit. The 1.5 μm slit (0.16 eV bandwidth) was used for spectroscopy and the 20 μm slit (2.2 eV bandwidth) for energy-filtered imaging. Bright field (BF) images were obtained by selecting the elastic (00) beam with a 20 μm diameter contrast aperture in the diffraction plane below the prism array, and loss images are available when the contrast aperture is placed on the loss signal ~35 μm (3.8 eV) away from the (00) beam.

Figure 1 shows a typical energy loss spectrum from a 6 μm diameter area on Ag(111), with an acquisition time of 1 s. The primary (nonloss) peak has a full width at half maximum (FWHM) of 0.30 eV. Assuming an energy spread of 0.25 eV for the incident cold field emission electron beam, the FWHM agrees with the expected spectrometer resolution of 0.16 eV. A prominent feature appears at a loss energy of 3.7–4.0 eV with apparent blue shift at larger parallel wave vectors, corresponding to the reported plasmon dispersions for both surface (3.69–4.12 eV) [16] and bulk (3.76–4.00 eV) [17] modes. Here we only consider the SP mode, because at the incident beam energy (E_I) of 19 eV used here [16,18] the bulk loss is ~10^2 times weaker than the surface. The FHWM of this loss feature is 0.37 eV, in good agreement with the width of our primary peak and the reported SP width (~0.2 eV) for Ag thin films [19]. Comparisons of the observed peak positions with previously reported SP dispersions of bulk [16] and thin film [19] Ag also exhibit very good agreement. These consistencies clearly demonstrate the excellent performance of the imaging spectroscopy method presented.

A quantitative analysis of SP peak intensities versus wave vector is presented in Fig. 2 for incident electron energies E_I of 19 and 53 eV. The theoretical probability of small-angle inelastic scattering by a surface dipole field can be written as [20]

$$\frac{d^3S}{dk_{\parallel}^2 d\hbar\omega} = \frac{m^2e^2|Q_{\parallel}(R_S + R_I) + i(R_I - R_S)\Delta k_z|^2}{\pi^2\hbar^4 k_I k_S \cos\theta_I \cos\theta_S Q_{\parallel}(Q_{\parallel}^2 + \Delta k_z^2)^2} \times \mathrm{Im}\left\{\frac{-1}{1 + \varepsilon_{\mathrm{eff}}(\omega, \mathbf{Q}_{\parallel})}\right\} \quad (1)$$

when $\hbar\omega/k_B$ is considerably higher than room temperature, where R_I and R_S represent the complex amplitude

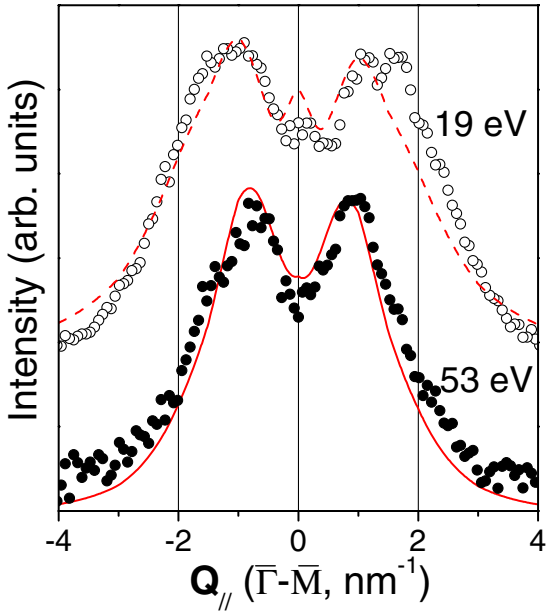

FIG. 2 (color online). $Q_\parallel$ dependence of the SP loss intensity for different incident electron energies E_I. Background is subtracted and the intensities are corrected for small irregularities in the slit width. The fits are obtained from Eq. (1), substituting R_I and R_S by $|R_I|$ and $|R_S|$, respectively, taking into account the width of the (00) beam and the effect of film thickness around $Q_\parallel = 0$.

reflectivity at the surface before and after the inelastic scattering. While there is no effective experimental method to determine the phase of these reflectivities, Eq. (1) can be simplified as

$$\frac{d^3S}{dk_\parallel^2 d\hbar\omega} = \frac{4m^2e^2Q_\parallel|R_I|^2}{\pi^2\hbar^4 k_I k_S \cos\theta_I \cos\theta_S (Q_\parallel^2 + \Delta k_z^2)^2} \times \mathrm{Im}\left\{\frac{-1}{1+\varepsilon_{\mathrm{eff}}(\omega, \mathbf{Q}_\parallel)}\right\} \quad (2)$$

when E_I is far from a reflectivity resonance energy [20]. The first term of Eq. (1) was calculated using experimental scattering conditions with R_I and R_S substituted by $|R_I|$ and $|R_S|$, experimentally available as the square root of the intensity reflectivity. The second term, known as the surface loss function, was calculated considering a $Q_\parallel$ dependent term in the free-electron polarization derived by the random phase approximation and surface perturbation induced by the distribution difference between free electrons and d-band dipoles [12], with the Ag dielectric function obtained from the optical constants shown in Ref. [21]. The finite film thickness (50 nm) was taken into account, which affects the peak intensity at $Q_\parallel = 0$. The calculated theoretical curves agree very well with the experimental intensities at the electron energies shown here. Thus, we find that we obtain high quality data on a small selected area, suitable for detailed quantitative analysis. Note that the data acquisition time of these Q-resolved spectra was only 1 sec., 3 to 4 orders of magnitude faster than traditional electron scattering experiments using a movable electron energy analyzer in which spectra at different Q are collected sequentially. Additionally, spectra of similar quality can be obtained on submicron areas by trading spatial resolution for data acquisition time. Data of similar quality can be obtained on a 0.5 μm diameter selected area by increasing the data acquisition time to 100 seconds. In contrast, traditional electron scattering experiments obtain E-Q spectra over areas with a typical diameter of $\sim$1 mm, further highlighting the advantages of LEEM based plasmon spectromicroscopy.

Figure 3 shows a set of energy-filtered images on a Ag(111)-Ag(100) combined island with corresponding no-loss BF LEEM, as well as PEEM images. The PEEM image (obtained with a Hg discharge lamp) [Fig. 3(a)] exhibits a distinctive contrast between Ag(111) and Ag(100), originating from the difference in the secondary electron emission efficiency [22]. BF and energy-filtered LEEM observations focus on the center of this island, which includes Ag(111), Ag(100), and Si(111)-($\sqrt{3}\times\sqrt{3}$)-Ag substrate areas. The BF LEEM image also exhibits prominent contrast between Ag(111) and Ag(100) at the electron energy of 52 eV [Fig. 3(b)] because the (00) beam reflectivity has a strong local maximum there on Ag(111), while it does not on Ag(100). The energy-filtered SP loss image exhibits similar contrast at the same beam energy [Fig. 3(c)], which is well explained by the intensity reflectivity term $|R_I|^2$ in Eq. (2). When the beam energy is reduced to 33 eV, the BF image loses the contrast between Ag(111) and Ag(100) [Fig. 3(d)], and the Ag(100) area becomes slightly more intense in the loss image [Fig. 3(e)]. It should be noted that the Si(111)-($\sqrt{3}\times\sqrt{3}$)-Ag area has some signal in the BF image, while it remains dark in the loss image at this beam energy, since the SP exists only on the island, and not on the surrounding Si substrate. The spatial resolution of these images is analyzed at 52 eV

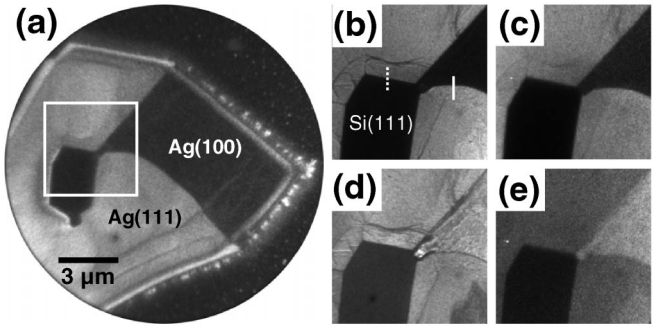

FIG. 3. (a) PEEM image of a Ag(111)-(100) composite island on Si(111). The Ag(111) domain appears brighter because of final state effects [23]. (b),(c) BF and plasmon loss LEEM images of the area shown as a solid square (a) at $E_I = 52$ eV. The boundaries at Ag(111)-Ag(001) (solid line) and Ag(111)-Si(111) (dotted line) are used to evaluate the resolution in this image (see text). (d),(e) Corresponding LEEM images at $E_I =$ 33 eV.

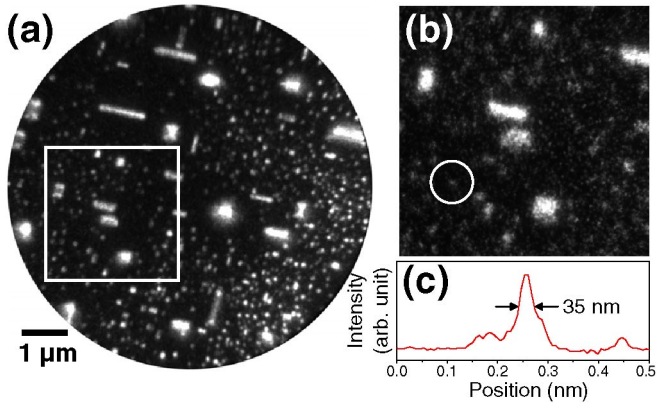

FIG. 4 (color online). (a) PEEM and (b) SP loss LEEM images ($E_I = 81$ eV) of Ag nanostructures on Si(001). The observation area in LEEM is shown as a solid square in (a). (c) One of the Ag nanoclusters marked by a solid circle in the SP loss LEEM image has a FWHM of 35 nm, close to the typical size of these clusters as measured with AFM.

[Figs. 3(b) and 3(c)]. The sharpest contrast edge at the boundary between Ag(111) and Si(111)-($\sqrt{3} \times \sqrt{3}$)-Ag gives 50 nm resolution. This is a reasonable value considering the finite resolution of the channel plate intensified phosphor screen [23], resulting in ~30 nm resolution at the image magnification used here, combined with large electrostatic field gradients at the edge of the tall island with ~50 nm thickness. The boundaries between Ag(111) and Ag(001) domains are imaged with ~100 nm resolution in the same BF image, reflecting its complex structure seen in Fig. 3(d). The resolution of the same boundary in the loss image is measured to be 110 nm, very similar to the BF image.

Ag nanostructures on Si(100) are shown in Fig. 4. Smaller nanoclusters with a typical lateral size of ~40 nm and ~7 nm thickness, as well as larger nanowires [24] with microns length and submicron width are seen in the conventional PEEM image [Fig. 4(a)]. The same nanowires and smaller clusters are also clearly imaged in the close-up loss image [Fig. 4(b)]. Some cluster images have lateral sizes of ~35 nm in FWHM [Fig. 4(c)], which can be explained by the phosphor screen resolution of 20 nm at the magnification range used here and cluster size of 30 nm. The excellent sensitivity and lateral resolution of energy-filtered LEEM demonstrated in this work will enable detailed nanoscale studies of nanocluster plasmons for molecular detection [5] and medical applications [6].

To conclude, an in-line energy filtering method for LEEM has been applied for observation of Ag surface plasmons. The SP dispersion on Ag(111) was measured with data collection efficiencies that are 3 to 4 orders of magnitude better than conventional electron scattering experiments. The spatial distribution of the SP loss signal was imaged on Ag(111) and Ag(001) domains, as well as on Ag nanostructures on Si(001) with an image resolution of less than 35 nm, in good agreement with the resolution expected for the image magnification employed in these experiments. Energy-filtered LEEM with the unique and superior performance presented here will serve as a powerful tool for both spatial and spectroscopic investigations of nanoplasmonics.

The authors gratefully acknowledge the contributions of James B. Hannon in the design and fabrication of the energy filter. The work by Y. F. and T. S. was supported by a Grant-in-Aid for Scientific Research from the Japan Society for the Promotion of Science.

[1] G. Mie, Ann. Phys. (Leipzig) **330**, 377 (1908).
[2] M. Fleischmann, P. J. Hendra and A. J. McQuillan, Chem. Phys. Lett. **26**, 163 (1974); M. Fleischmann, P. J. Hendra, and A. J. McQuillan, J. Chem. Soc. Chem. Commun. **3**, 80 (1973).
[3] W. L. Barnes, A. Dereux and T. W. Ebbesen, Nature (London) **424**, 824 (2003).
[4] E. Ozbay, Science **311**, 189 (2006).
[5] S. Nie and S. R. Emory, Science **275**, 1102 (1997).
[6] L. R. Hirsch *et al.*, Proc. Natl. Acad. Sci. U.S.A. **100**, 13549 (2003).
[7] P. Dawson, F. de Fornel and J.-P. Goudonnet, Phys. Rev. Lett. **72**, 2927 (1994); B. Hecht *et al.*, Phys. Rev. Lett. **77**, 1889 (1996).
[8] R. Berndt and J. K. Gimzewski, Phys. Rev. B **48**, 4746 (1993); M. Sakurai and M. Aono, Phys. Rev. B **64**, 045402 (2001).
[9] A. Kubo *et al.*, Nano Lett. **5**, 1123 (2005); A. Kubo, N. Pontius, and H. Petek, Nano Lett. **7**, 470 (2007).
[10] R. F. Egerton, *Electron Energy-Loss Spectroscopy in the Electron Microscope* (Plenum, New York, 1986) and references therein.
[11] P. E. Batson, Phys. Rev. Lett. **49**, 936 (1982); Surf. Sci. **156**, 720 (1985).
[12] A. Liebsch, Phys. Rev. Lett. **71**, 145 (1993); A. Liebsch and W. L. Schaich, Phys. Rev. B **52**, 14 219 (1995).
[13] E. Bauer *et al.*, J. Electron Spectrosc. Relat. Phenom. **84**, 201 (1997); E. Bauer, *ibid.* **114–116**, 975 (2001).
[14] R. Tromp *et al.*, Surf. Rev. Lett. **5**, 1189 (1998).
[15] R. M. Tromp *et al.* (to be published).
[16] S. Suto *et al.*, Phys. Rev. Lett. **63**, 2590 (1989).
[17] P. Zacharias and K. L. Kliewer, Solid State Commun. **18**, 23 (1976).
[18] M. Rocca and U. Valbusa, Phys. Rev. Lett. **64**, 2398 (1990).
[19] Y. H. Yu *et al.*, Phys. Rev. B **72**, 205405 (2005).
[20] H. Ibach and D. L. Mills, *Electron Energy Loss Spectroscopy and Surface Vibrations* (Academic, New York, 1982), p. 71; E. Evans and D. L. Mills, Phys. Rev. B **5**, 4126 (1972).
[21] E. D. Palik, *Handbook of Optical Constants of Solids* (Academic, New York, 1985), p. 350.
[22] A. Otto and B. Reihl, Phys. Rev. B **41**, 9752 (1990).
[23] H. Shimizu, T. Yasue, and T. Koshikawa (private communications).
[24] J. Tersoff and R. M. Tromp, Phys. Rev. Lett. **70**, 2782 (1993).